# Osmotic Flow in Porous Membranes : Effects of Electric Charge

Takeshi AKINAGA, Masako SUGIHARA-SEKI and Tomoaki ITANO

*Department of Pure and Applied Physics, Faculty of Engineering Science, Kansai University, Suita, Osaka*

The electrostatic model for osmotic flow across a porous membrane in our previous study (Akinaga et al. 2008)[1] was extended to include the streaming potential, for solutes and pores of like charge and fixed surface charge densities. The magnitude of the streaming potential was determined to satisfy zero current condition along the pore axis. It was found that the streaming potential affects the velocity profiles of the pressure driven flow as well as the osmotic flow through the pore, and decreases their flow rates, particularly in the case of large Debye length relative to the pore radius, whereas it has little effect on the reflection coefficients of spherical solutes through cylindrical pores.

## 1. INTRODUCTION

Osmotic flow is generated between solutions of different concentrations separated by a porous membrane. In the thermodynamic approach the volume flux of the solution, $J_v$, can be approximately expressed in terms of the pressure difference $\Delta p_\infty$ and the osmotic pressure difference $\Delta\pi_\infty$ across the membrane:

$$J_v = L_p(\Delta p_\infty - \sigma\Delta\pi_\infty), \tag{1}$$

where the coefficient $L_p$ is called the hydraulic conductivity and $\sigma$ is the reflection coefficient [2]. For a semi-permeable membrane where the solute radius is larger than the pore radius, $\sigma = 1$. When the solute radius is smaller than the pore radius, i.e. the membrane is leaky, $\sigma < 1$. The reflection coefficient is known to be a relevant measure of the magnitude of possible osmotic flow across membranes [3,4].

Osmotic phenomena through leaky porous membranes are of great biological significance. In particular, osmosis across the epithelial or endothelial cell layers lining the kidney tubules, blood capillaries, intestines and other internal body organs plays a critical role in their transport properties [3-5]. In the measurements of the material transport in such organs, significant contributions of electric charge or charge selective properties have been often reported. For example, it has been long known that transport of polyanions across glomerular capillary walls is substantially reduced and that of polycations enhanced, compared to the transport of neutral macromolecules of comparable size and structure [5]. The reflection coefficient measured for anionized myoglobin across blood capillary walls was much larger than that for neutral myoglobin [6].

The simplest way to describe such charge effects is to model the solute of interest as a point charge and to assume an equilibrium relationship between the membrane and adjacent solutions. This model, called the Donnan-type model, was widely used to account for the charge selectivity of glomerular and microvascular

permeability [3-5]. Sasidhar & Ruckenstein [7] examined osmotic flow due to difference in electrolyte concentration, by using a diffuse double-layer model. In the model, the ions were assumed to be point charges. Recently, Stace & Damiano [8] considered the electrochemical dynamics of anionic molecular transport within blood capillaries, by modeling the endothelial surface glycocalyx as a continuously distributed anionic matrix containing fixed–bound negative charges.

The effect of finite size of solute on osmotic flow was considered by Anderson & Malone [9], in the case of neutral solutes flowing through leaky porous membranes. Before their work, Mauro [10] and Ray [11] proposed an idea of local equilibrium at each end of a long pore to describe the driving mechanism of osmotic flow for semi-permeable membranes. Anderson & Malone [9] extended the idea of local osmotic equilibrium to leaky membranes: When solutes with radius $a$ enter a circular cylindrical pore, their centers are excluded from a region of thickness $a$ next to the pore wall. This radial concentration decrease would create a radial pressure drop toward the pore wall, if the equilibrium condition of $p - \pi =$ constant is realized in the radial direction, where $p$ and $\pi$ are the hydrostatic and osmotic pressures. Since the solute concentration or $\pi$ varies along the pore axis, this radial pressure drop will give rise to an axial pressure gradient at least near the pore wall, which drives the osmotic flow. Based on this idea, Anderson & Malone analyzed osmotic flow across a membrane with circular cylindrical pores and calculated the reflection coefficient of spherical solute as a function of the solute radius relative to the pore radius.

Recently, the idea of Anderson & Malone was used to estimate the reflection coefficient of neutral solutes for the endothelial surface glycocalyx of microvessels [12]. Yan et al. [13] examined the effect of pore entrance and exit for neutral solutes. They found that for permeable membranes there are fine-scale entrance/exit regions of a few pore radii from the pore openings where the solute concentrations are different from the far-field values. It was reported that this effect on the reflection coefficient is insignificant although it may affect the osmotic flux to some extent for small solutes and short pores.

In our previous study [1], we extended the Anderson-Malone model to include electrostatic effects, for the case that the surfaces of the pore wall and the solutes have prescribed electrical charges with the same sign and the solute and pore radii are comparable. The suspending fluid was assumed to be an electrolyte in which ions are regarded as point charges. Due to repulsive electrostatic interaction between the surface charges, the solutes are more likely to be excluded from the pore wall. As a result, the osmotic flow through the pore was found to be significantly enhanced even for a small Debye length relative to the pore radius, compared to no-charged case. We herein refer to this study as ref. 1.

In ref. 1, we assumed that the reservoirs on both sides of the membrane are large enough that the electric current generated by the convection through the pore does not affect the osmotic flow. However, if this condition is not satisfied, i.e. the reservoirs are not large enough that accumulations of electric charges due to the electric current in the reservoirs can not be neglected, then this accumulation will generate a potential gradient along the pore axis that opposes the mechanical transfer of charge. Since the potential gradient induces the migration of ions, the equilibrium state may be such that the current due to ion migration generated by the potential gradient balances that due to convection. In this case, we must impose zero net current condition along the pore axis. The potential at the equilibrium condition to satisfy the zero current condition is termed the streaming potential [14].

In the present study, we include the streaming potential in our model in ref. 1, and examine its contribution to the osmotic flow across a membrane with long circular cylindrical pores with specified surface charges.

## 2. MODEL AND FORMULATION

### 2.1 Assumptions

We consider osmotic flow across a membrane with long circular cylindrical pores (figure 1). On both sides of the membrane, there are two solutions differing in solute concentration $\Delta c_\infty$ and in hydrostatic pressure $\Delta p_\infty$. The length of the pore or the width of the membrane, $L$, is assumed to be much larger than the pore radius $r_c$, i.e. $l = L/r_c >> 1$. The surface of the pore has uniformly distributed electric charge with density $q_c$. The solutes are identical rigid spheres (radius $a$) with uniformly distributed surface charge (density $q_s$), and they are suspended in

an electrolyte. The solution is assumed to be dilute enough that the interaction between the solutes can be neglected [15].

The sizes of ions in the electrolyte are assumed to be small compared to both of solute radius and pore radius. Thus, we adopt a point-charge description for the ions and the electrolyte is regarded as an incompressible Newtonian fluid with viscosity $\mu$. The bulk electrolyte concentrations on both sides of the membrane are taken to be equal, so that osmosis results only from an imbalance in solute concentrations, i.e. $\Delta\pi_\infty = RT\Delta c_\infty$, where $R$ is the gas constant and $T$ is the absolute temperature. The temperature is assumed be constant in the current study.

The Reynolds numbers which pertain to flow through macromolecular dimensions are extremely small, so that we neglect inertia forces in fluid and solute motions. For low Reynolds number flows, hydrodynamic entrance lengths as well as the length scale for the concentration transitions at the pore ends are estimated to be on the order of the pore radius [13,16]. Thus, we neglect hydrodynamic end effects and apply equilibrium conditions at the pore ends, from the assumption of long pores ($L >> r_c$). It is also assumed that the Peclet number defined in terms of the pore radius and fluid mean velocity is small enough, so that radial variations in solute concentration closely resemble those at equilibrium, despite the axial variations caused by differing external concentrations [16,17]. We also assume the radial equilibrium for ions in the electrolyte in the pore.

In the next section, we briefly review the formulation for the osmotic flow in the absence of the streaming potential, and then we modify it, by taking the streaming potential into account.

## 2.2 Osmotic flow model

We take the cylindrical coordinates ($r$, $\varphi$, $z$) with the $z$-axis along the centerline of the pore. From axi-symmetric configuration, we denote the fluid velocity as $\boldsymbol{u} = (u_r, 0, u_z)$, the hydrostatic pressure as $p(r, z)$, the solute concentration as $c = c(r, z)$, and the potential for the solute as $\phi(r, z)$. The solute potential $\phi(r, z)$ is defined relative to the bulk phase where its value is zero. In the absence of the streaming potential that is the case considered in ref. 1, the Stokes equation is expressed as

$$-\nabla p + \mu\nabla^2 \boldsymbol{u} - c\nabla\phi - \rho_e\nabla\psi = 0, \tag{2}$$

where $\rho_e$ is the charge density of ions in the electrolyte and $\psi(r)$ is the double-layer potential obtained in ref. 1. Since the cross-section of the pore is uniform and the length $L$ is much larger than the pore radius, we assume that $|u_z| >> |u_r|$ and $\phi = \phi(r)$. Under these assumptions, we obtain the simplified equation for the axial velocity from equation (2):

$$-\frac{\partial p}{\partial z} + \mu\frac{1}{r}\frac{\mathrm{d}}{\mathrm{d}r}\left(r\frac{\mathrm{d}}{\mathrm{d}r}\right)u_z = 0. \tag{3}$$

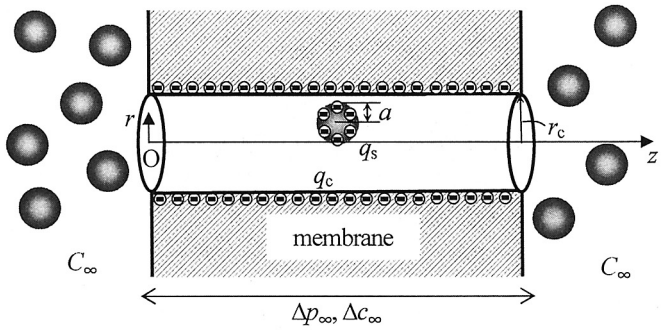


Fig. 1 A sketch of osmotic flow across a membrane with long circular cylindrical pores with radius $r_c$ and length $L$ ($l = L/r_c >> 1$). Spherical solutes with radius $a$ are suspended in an electrolyte. The surfaces of the pore wall and the solutes are electrically charged with density $q_c$ and $q_s$, respectively. On both sides of the membrane, there are two solutions differing in solute concentration $\Delta c_\infty$ and in hydrostatic pressure $\Delta p_\infty$. The concentrations of monovalent cation and anion are $C_\infty$ in bulk solution.

The radial component of equation (2) leads to the approximate equation:

$$\frac{\partial p}{\partial r} + c\frac{\mathrm{d}\phi}{\mathrm{d}r} + \rho_e \frac{\mathrm{d}\psi}{\mathrm{d}r} = 0. \tag{4}$$

From the assumption of the radial equilibrium for the solutes, we have the Boltzmann distribution for the solute concentration $c(r, z)$:

$$c(r,z) = c_0(z)\exp[-\frac{\phi(r)-\phi_0}{RT}], \tag{5}$$

where the subscript 0 indicates the values on the $z$-axis. Substitution of equation (5) into equation (4) and subsequent integration yields

$$p(r,z) = p_0(z) - \pi_0(z)\{1 - e^{-(\phi(r)-\phi_0)/RT}\} - \int_0^r \rho_e \frac{\mathrm{d}\psi}{\mathrm{d}r}\mathrm{d}r, \tag{6}$$

where $\pi_0(z) = RTc_0(z)$ represents the osmotic pressure along the $z$-axis[9]. Equation (6) illustrates the coupling among solute concentration, ion concentration and pressure which generates the driving force for bulk flow.

The solution $u_z(r)$ of equation (3) with the pressure given by equation (6) provides the velocity profile in the pore. Here, using a characteristic velocity in the pore $U$, we introduce dimensionless quantities, such as $r^* = r/r_c$, $z^* = z/r_c$, $u^* = u_z/U$, $p^* = p\,(r_c/\mu U)$, $\phi^* = \phi/RT$, and $\pi^* = \pi\,(r_c/\mu U)$, and we rewrite the preceding equations in dimensionless forms.

Substituting dimensionless version of equation (6) into that of equation (3) leads to

$$\frac{1}{r^*}\frac{\mathrm{d}}{\mathrm{d}r^*}(r^*\frac{\mathrm{d}}{\mathrm{d}r^*})u^* = p_0^{*\prime} - \pi_0^{*\prime} + \pi_0^{*\prime} e^{-(\phi^*(r^*)-\phi_0^*)}, \tag{7}$$

where the prime represents d/dz*. Since this equation is linear in $u^*$, its solution $\bar{u}^*(r^*)$ satisfying the no-slip condition on the pore wall can be expressed in the form that

$$\bar{u}^*(r^*) = -p_0^{*\prime}u_1^* + \pi_0^{*\prime}(u_1^* - u_2^*), \tag{8}$$

where $u_1^*$ and $u_2^*$ satisfy

$$\frac{1}{r^*}\frac{\mathrm{d}}{\mathrm{d}r^*}(r^*\frac{\mathrm{d}}{\mathrm{d}r^*})u_1^* = -1, \quad \frac{1}{r^*}\frac{\mathrm{d}}{\mathrm{d}r^*}(r^*\frac{\mathrm{d}}{\mathrm{d}r^*})u_2^* = -e^{-(\phi^*(r^*)-\phi_0^*)}. \tag{9a,b}$$

They are explicitly expressed as

$$u_1^*(r^*) = \frac{1-r^{*2}}{4}, \quad u_2(r^*) = \int_{r^*}^1 \frac{\mathrm{d}y}{y}\int_0^y x e^{-(\phi^*(x)-\phi_0^*)}\mathrm{d}x. \tag{10a, b}$$

Equation (10a) represents the Poiseuille flow. In general, the profile of the flow (10b) is not parabolic for leaky membranes. By integrating equation (8) over the cross-section of the pore, we have the flux through the pore, $\bar{U}^*$, as

$$\bar{U}^* = -p_0^{*\prime}U_1^* + \pi_0^{*\prime}(U_1^* - U_2^*), \tag{11}$$

where

$$U_1^* = \frac{1}{\pi}\int_0^1 u_1^* 2\pi r\,\mathrm{d}r = \frac{1}{8}, \quad U_2^* = 2\int_0^1 r\mathrm{d}r\int_r^1 \frac{\mathrm{d}y}{y}\int_0^y x e^{-(\phi^*(x)-\phi_0^*)}\mathrm{d}x. \tag{12a, b}$$

## 2.3 Streaming potential

In the present study, we include a streaming potential $\psi^s$ to impose the condition of zero current along the $z$-axis. In this case, the body force resulting from the Coulomb force $-\rho_e \partial\psi^s/\partial z$ must be added to equation

(3). Here, the charge density of ions is given by $\rho_e = F(z_+C_+ + z_-C_-)$, where $F$ is Faraday's constant, and $z_\pm$, $C_\pm$ are valences and concentrations of ions, respectively. From the assumption of the radial equilibrium for ions, their concentrations are given by [15]

$$C_\pm = C_{0\pm} \exp[-Fz_\pm\psi / RT], \tag{13}$$

where $\psi$ is the double-layer potential for a pore with constant surface charge $q_c$. The condition of charge neutrality of the whole system is expressed as

$$z_+C_{0+} + z_-C_{0-} = 0. \tag{14}$$

Similarly to ref. 1, we consider only the case of $z_+ = -z_- = 1$ and $C_{0\pm} = C_\infty$. Thus, the charge density is expressed as

$$\rho_e = -2FC_\infty \sinh(F\psi / RT). \tag{15}$$

Instead of equation (3), the momentum equation becomes in a dimensionless form:

$$-\frac{\partial p^*}{\partial z^*} + \frac{1}{r^*}\frac{d}{dr^*}(r^*\frac{d}{dr^*})u^* + \beta \sinh\psi^* \frac{\partial \psi^{s*}}{\partial z^*} = 0, \tag{16}$$

where $\beta = 2C_\infty r_c RT / \mu U$ and we have defined dimensionless electric potentials $\psi^* = F\psi / RT$ and $\psi^{s*} = F\psi^s / RT$.

Corresponding to equation (7), substitution of equation (6) into equation (16) yields

$$\frac{1}{r^*}\frac{d}{dr^*}(r^*\frac{d}{dr^*})u^* = p_0{}^{*\prime} - \pi_0{}^{*\prime} + \pi_0{}^{*\prime} e^{-(\phi^*(r^*)-\phi_0^*)} - \beta\psi^{s*\prime}\sinh\psi^*. \tag{17}$$

and its solution is given by

$$u^*(r^*) = \bar{u}^*(r^*) + \beta\psi^{s*\prime}u^{s*}(r^*), \tag{18}$$

where

$$u^{s*}(r^*) = \int_{r^*}^{1}\frac{dy}{y}\int_0^y x\sinh\psi^*(x)\,dx. \tag{19}$$

Similarly to equation (11), the dimensionless flux $U^*$ through the pore can be expressed as

$$U^* = \bar{U}^* + \beta\psi^{s*\prime}U^{s*} = -p_0{}^{*\prime}U_1{}^* + \pi_0{}^{*\prime}(U_1{}^* - U_2{}^*) + \beta\psi^{s*\prime}U^{s*}, \tag{20}$$

where

$$U^{s*} = 2\int_0^1 r\,dr\int_r^1\frac{dy}{y}\int_0^y x\sinh\psi^*(x)\,dx. \tag{21}$$

## 2.4 Zero current condition

Let us consider the electric current along the $z$-axis, which is given in the dimensional form by [14]

$$i(r) = \rho_e u_z(r) + (F^2/RT)(C_+D_+ + C_-D_-)(-d\psi^s/dz). \tag{22}$$

Here, $D_\pm$ are the diffusion constants for cation and anion, and we assume $D_+ = D_- = D$, for simplicity. The first term on the right-hand-side of equation (22) represents the current created by the convection and the second term from the migration induced by the electric field. Adopting equation (13) and introducing dimensionless current $i^* = i / 2FC_\infty U$, the current in a dimensionless form is simplified to

$$-i^* = u^*(r^*)\sinh\psi^* + \gamma\psi^{s*\prime}\cosh\psi^*, \tag{23}$$

where $\gamma = D/r_cU$. Substitution of equation (18) into equation (23) yields

$$-i^* = \bar{u}^*(r^*)\sinh\psi^* + \{u^{s*}(r^*)\sinh\psi^* + (\gamma/\beta)\cosh\psi^*\}\beta\psi^{s*\prime}. \tag{24}$$

By integrating equation (24) over the cross-section of the pore to obtain the total current and equating that to zero, we have

$$\beta\psi^{s*\prime} = -\frac{\int_0^1 \bar{u}^*(r)\sinh\psi^* r\mathrm{d}r}{\int_0^1 \{u^{s*}(r)\sinh\psi^* + (\gamma/\beta)\cosh\psi^*\} r\mathrm{d}r}. \tag{25}$$

This equation determines the gradient of the streaming potential, which has the form of $\beta\psi^{s*\prime} = p_0^{*\prime}A - \pi_0^{*\prime}B$, as evident from equation (8). Here, $A$ and $B$ are given by

$$A = \frac{1}{C}\int_0^1 u_1^*(r)\sinh\psi^* r\mathrm{d}r,\ B = \frac{1}{C}\int_0^1 (u_1^*(r) - u_2^*(r))\sinh\psi^* r\mathrm{d}r, \tag{26}$$

where $C$ is the denominator of equation (25).

## 2.5 Reflection coefficient

Substitution of $\beta\psi^{s*\prime} = p_0^{*\prime}A - \pi_0^{*\prime}B$ into equations (18) and (20) gives

$$u^*(r^*) = -p_0^{*\prime}(u_1^* - Au^{s*}) + \pi_0^{*\prime}(u_1^* - u_2^* - Bu^{s*}), \tag{27}$$

and

$$U^* = -p_0^{*\prime}(U_1^* - AU^{s*}) + \pi_0^{*\prime}(U_1^* - U_2^* - BU^{s*}). \tag{28}$$

Since $U^*$ is constant independent of $z^*$ by continuity condition, then one can integrate equation (28) along the $z$-axis from the entrance ($z^* = 0$) to the exit ($z^* = l$) to obtain

$$U^* = \frac{U_1^* - AU^{s*}}{l}\{(p_0^*(0) - p_0^*(l)) - (\pi_0^*(0) - \pi_0^*(l))\frac{U_1^* - U_2^* - BU^{s*}}{U_1^* - AU^{s*}}\}. \tag{29}$$

The Boltzmann and Gibbs-Duhem relations are applied at the pore ends [9]:

$$\pi_0^*(0) = \pi_{0\infty}^* e^{-\phi_0^*},\ \pi_0^*(l) = \pi_{l\infty}^* e^{-\phi_0^*},$$
$$p_0^*(0) = p_{0\infty}^* - \pi_{0\infty}^*(1 - e^{-\phi_0^*}),\ p_0^*(l) = p_{l\infty}^* - \pi_{l\infty}^*(1 - e^{-\phi_0^*}), \tag{30}$$

where $p_{0\infty}^*$, $p_{l\infty}^*$, $\pi_{0\infty}^*$, and $\pi_{l\infty}^*$ are all dimensionless quantities in bulk fluid phase at the entrance and the exit of the pore (see figure 1). By the use of the dimensional values $\Delta p_\infty = (\mu U/r_c)(p_{0\infty}^* - p_{l\infty}^*)$ and $\Delta\pi_\infty = (\mu U/r_c)(\pi_{0\infty}^* - \pi_{l\infty}^*)$, equation (29) is finally reduced to equation (1) for the dimensional flux $J_v$:

$$J_v = \alpha U U^* = L_p(\Delta p_\infty - \sigma\Delta\pi_\infty), \tag{31}$$

where

$$L_p = \frac{\alpha r_c^2}{\mu L}(U_1^* - AU^{s*}),\quad \sigma = 1 - \frac{U_2^* - (A-B)U^{s*}}{U_1^* - AU^{s*}}e^{-\phi_0^*}, \tag{32a, b}$$

and $\alpha$ is the void fraction of the membrane. If we substitute the expressions for $U_1^*$, $U_2^*$ and $U^{s*}$ into equation (32b), we can evaluate the values of $\sigma$.

In the absence of the streaming potential that is the case considered in ref. 1, equations (32a) and (32b) lead to

$$L_p^0 = \alpha r_c^2/8\mu L,\quad \sigma^0 = 1 - 8U_2^* e^{-\phi_0^*} = 1 - 16\int_0^1 r\mathrm{d}r\int_r^1 \frac{\mathrm{d}y}{y}\int_0^y x e^{-\phi^*(x)}\mathrm{d}x. \tag{33a, b}$$

The superscript 0 in equations (33a) and (33b) indicates the values in the absence of the streaming potential. The latter coincides with equation (2) in ref. 1.

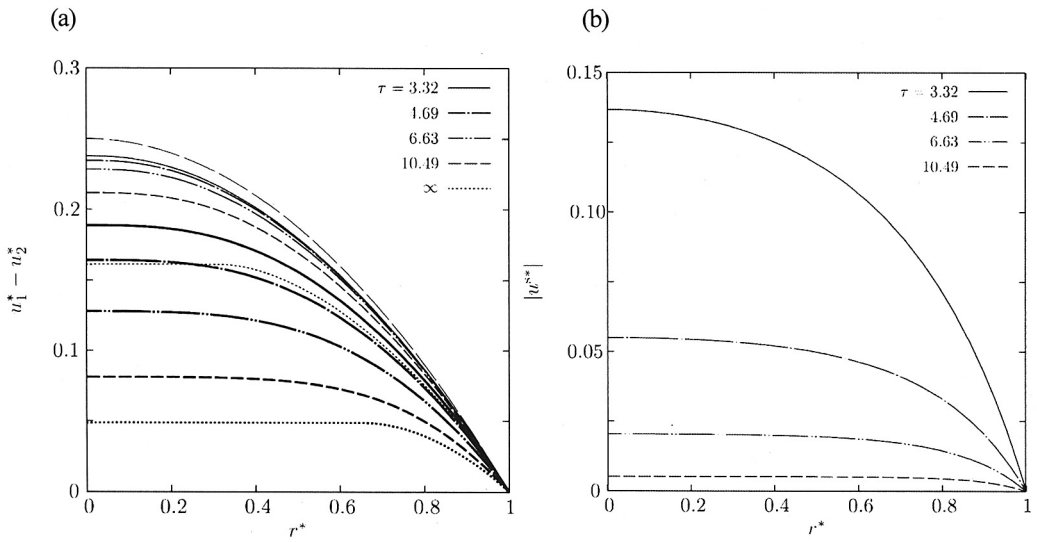


Fig. 2 (a) Dimensionless velocity profiles of the osmotic flow, $u_1$*- $u_2$*, in the absence of the streaming potential, for various values of $\tau$ at $q_s$*= $q_c$*= -5.70. The thick curves represent the cases of $a^*$ = 0.333 and the thin curves $a^*$ = 0.667. For reference, the Poiseuille flow $u_1$* (equation (10a)) is plotted by a dashed curve, corresponding to $u_1$*- $u_2$* in the limit of $a^*$ → 1. (b) Dimensionless velocity profiles $|u^{s*}|$ induced by the streaming potential for various values of $\tau$ at $q_c$*= -5.70.

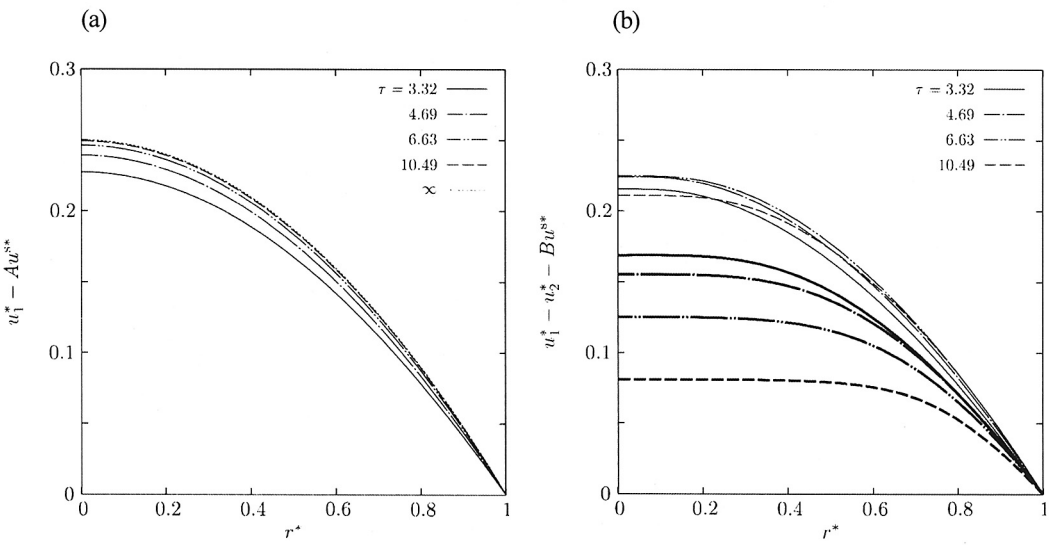


Fig. 3 Dimensionless velocity profiles (a) $u_1$*-$Au^{s}$* and (b) $u_1$*-$u_2$*-$Bu^{s}$*, which are proportional to the pressure gradient and the osmotic pressure, respectively (see equation (27)), for various values of $\tau$ at $q_s$*= $q_c$*= -5.70. In (a), the Poiseuille flow is plotted by a dotted curve, corresponding to $u_1$*- $Au^{s}$* in the limit of $\tau \rightarrow \infty$. In (b), the thick curves represent the cases of $a^*$ = 0.333 and the thin curves $a^*$ = 0.667.

2.6 Parameters

In ref. 1, we have estimated σ from equation (33b) for various values of $a$, $q_s$, $q_c$ and $C_\infty$ at $r_c$= 10 nm and $T$= 310 K, in the case of repulsive interaction, in other words, $q_s$ and $q_c$ having the same sign. In the present study, we also focus on the case of like charge and $r_c$= 10 nm, $T$= 310 K. Specifically, we set $q_s$ and $q_c$ both negative. The results obtained are easily applied to the other case of $q_s$ and $q_c$ both positive.

We define the Debye length, which is expressed for a univalent-univalent electrolyte as

$$\lambda_D = [\varepsilon RT / 2F^2 C_\infty]^{1/2}, \tag{34}$$

where $\varepsilon$ is the electric permittivity. Note that $\lambda_D \approx 1$ nm for a 0.1 M aqueous solution at $T$ = 310 K. The ratio of the pore radius and the Debye length, $\tau = r_c/\lambda_D$, provides an important parameter in the current problem. Other dimensionless parameters involved are the size ratio $a^* = a/r_c$, dimensionless surface charges $q_c^* = q_c r_c F/\varepsilon RT$, $q_s^* = q_s r_c F/\varepsilon RT$ and $\gamma/\beta = \mu D/2C_\infty r_c^2 RT = \{\mu D F^2/\varepsilon (RT)^2\}/\tau^2$ appeared in equation (25). The charge densities $q_c$ (or $q_s$) = $-5\times10^{-3}$ C/m$^2$ and $-1\times10^{-2}$ C/m$^2$ considered in ref. 1 corresponds to $q_c^*$ (or $q_s^*$) = -2.85 and -5.70, respectively. Corresponding to aqueous NaCl solutions at 310 K, we set $D = 2.2\times10^{-9}$ m$^2$/s, $\mu = 0.69\times10^{-3}$ Pa. s, and $\varepsilon = 6.57\times10^{-10}$ C$^2$/N m$^2$ to obtain $\gamma/\beta = 3.24/\tau^2$.

2.7 Methods

We have analyzed the double-layer potential $\psi^*$ ($r^*$) based on a mean-field theory, and computed the interaction energy $\phi^*$ ($r^*$) in ref. 1. In the current study, the obtained values of $\psi^*$ ($r^*$) and $\phi^*$ ($r^*$) were used to compute the velocity profiles of $u_2^*(r^*)$ and $u^{s*}(r^*)$, and to estimate its contribution to the reflection coefficient σ, for various values of $\tau$ and $a^*$ at some representative charge densities $q_c^*$ and $q_s^*$.

The numerical calculations were carried out by utilizing the spectral element method [1]. The electric potential and the flow velocities appeared in equations (10b), (12b), (19) and (21) and (26) were expanded by 12th-order Lagrangian interpolants. The integrations were performed by employing the Gauss-Legendre quadrature procedure of 24th degree.

## 3. RESULTS AND DISCUSSION

The velocity profiles of $u_1^* - u_2^*$ and $|u^{s*}|$ are plotted in figure 2. The former represents the osmotic flow in the absence of the streaming potential as seen in equation (8), and the latter is the flow induced by the streaming potential. Note that $u^{s*}$ is negative, because the pore wall is negatively charged in the current study. Since the osmotic flow $u_1^* - u_2^*$ is generated by a driving force near the pore wall which results from the exclusion of solutes, it has a blunter profile compared to the Poiseuille flow, and this trend is more enhanced for smaller solutes. Similarly, the magnitude of the driving force for $u^{s*}$ increases with radial position $r^*$ as $|\sinh\psi^*(r^*)|$, so that its profile is also blunter than the Poiseuille flow. Figures 2(a) and (b) show that both of $u_1^* - u_2^*$ and $|u^{s*}|$ increase with decreasing τ. Since electrostatic interaction is larger for smaller τ, this result indicates that the repulsive electrostatic interaction between solute and pore surface charges enlarges the osmotic flow as well as the flow due to the streaming potential.

In the presence of the streaming potential, the pressure driven flow and the osmotic flow are given by $u_1^* - Au^{s*}$ and $u_1^* - u_2^* - Bu^{s*}$, respectively, while the corresponding velocities are $u_1^*$ and $u_1^* - u_2^*$, in the absence of the streaming potential. The velocity profiles of $u_1^* - Au^{s*}$ and $u_1^* - u_2^* - Bu^{s*}$ are plotted in figures 3(a) and (b), for some representative cases. Figure 3(a) shows that the pressure driven flow diminishes with decreasing τ, while it is independent of τ in the absence of the streaming potential. A comparison of figures 2(a) and 3(b) indicates that the osmotic flow decreases when the streaming potential is generated. Since both of $u_1^* - u_2^*$ and $Bu^{s*}$ monotonically increase with decreasing τ, $u_1^* - u_2^* - Bu^{s*}$ varies with τ in a complicated manner, as seen from the curves for $a^*$=0.667 in figure 3(b). However, it is evident, in general, that the effect of the streaming potential is larger for smaller τ.

The obtained values of the reflection coefficient σ are plotted in figure 4 as a function of the size ratio $a^*$ at τ =3.32, 4.69, 6.63 and 10.5, corresponding to the ion concentration $C_\infty$=0.01, 0.02, 0.04 and 0.10 M. For

comparison, the reflection coefficient $\sigma^0$ in the absence of the streaming potential is also plotted by small closed circles for the same parameter values. Surprisingly, the values of the reflection coefficients in the two cases coincide remarkably with each other for all cases examined. As a result, the difference between the two values $\sigma$ and $\sigma^0$ can not be notable in figure 4. This result is quite interesting because the velocity profiles in the pore are affected by the streaming potential as seen in figure 3, whereas it has little effect on the reflection coefficients.

It is hard to prove analytically the coincidence of the reflection coefficients with and without the streaming potential shown in figure 4. Here, we consider two extreme cases of $a^* \to 0$ and 1. For $a^* \ll 1$, it is evident that $\phi_0^* \approx 0$. It is also shown that $U_1^* \approx U_2^*$ and $B \approx 0$, since $u_1^*(r^*) \approx u_2^*(r^*)$. Thus, equation (32b) yields that $\sigma \approx \sigma^0 \approx 0$ in this case. In the other limit of $a^* \to 1$, it is seen that $u_2^*(r^*) \approx 0$, so that $U_2^* \approx 0$ and $A - B \approx 0$. Thus, it is concluded that $\sigma \approx \sigma^0 \approx 1$ in this case.

So far, we have reported the results only for the case of $q_c^* = q_s^* = -5.70$. In ref. 1, we treated four cases of $(q_c^*, q_s^*) = (-5.70,-5.70), (-5.70,-2.85), (-2.85,-5.70)$, and $(-2.85,-2.85)$. In all cases examined, the results reported here are qualitatively unchanged, and the electrostatic effects are enlarged for larger charge densities, as may be expected.

## 4. CONCLUDING REMARKS

We have developed an electrostatic model for osmotic flow across a porous membrane, including the effect of the streaming potential. It was found that the streaming potential decreases the pressure driven flow as well as the osmotic flow, but it has little effects on the reflection coefficients for the parameter range examined.

**Acknowledgement** This research has been supported in part by a Grand-in-Aid for Scientific Research (B) 19360090 and by Kansai University Special Research Fund, 2009.

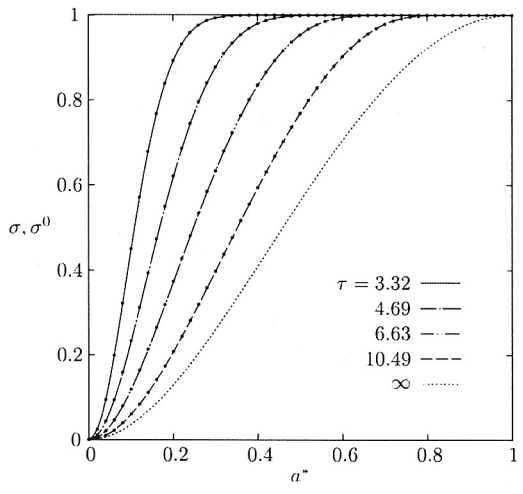


Fig. 4 Osmotic reflection coefficients $\sigma$ and $\sigma^0$ as a function of $a^*$ for various values of $\tau$ at $q_s^* = q_c^* = -5.70$. The curves represent $\sigma$ and closed circles represent $\sigma^0$. For reference, the reflection coefficients for steric condition alone, corresponding to $\sigma$ in the limit of $\tau \to \infty$, are plotted by a thin dotted curve.

## REFERENCES


1) Akinaga, T., Sugihara-Seki, M., and Itano, T., "Electrical charge effect on osmotic flow through pores", *J. Phys. Soc. Jpn* 77, (2008), pp.053401-1 - 053401-4.
2) Kedem, O. and Katchalsky, A., "Thermodynamic analysis of the permeability of biological membranes to non-electrolytes", *Biochem. Biophys. Acta* 27, (1958), pp.229-246.
3) Curry, F.E., "Mechanics and thermodynamics of transcappillary exchange", In: Handbook of Physiology (Am. Physiol. Soc. 1984), vol. 4 part 1, pp. 309-374.
4) Michel, C.C. and Curry, F.E., "Microvascular permeability", *Physiol. Rev.* 79, (1999), pp.703-761.
5) Haraldsson, B., Nystrom, J. and Deen, W.M., "Properties of the glomerular barrier and mechanisms of proteinuria", *Physiol. Rev.* 88, (2008), pp.451-487.
6) Michel, C.C. and Turner, M.R. "The effects of molecular charge on the permeability of frog mesenteric capillaries to myoglobin", *J. Physiol. Lond.* 316, (1981), pp.51-52.
7) Sasidhar, V. and Ruckenstein, E., "Electrolyte osmosis through capillaries", *J. Colloid Interface Sci.* 82, (1981), pp.439-457.
8) Stace, T.M. and Damiano, E.R., "An electrochemical model of the transport of charged molecules through the capillary glycocalyx", *Biophys. J.* 80, (2001), pp.1670-1690.
9) Anderson, J.L. and Malone, D.M., "Mechanism of osmotic flow in porous membranes", *Biophys J.* 14, (1974), pp. 957-982.
10) Mauro, A., "Nature of solvent transfer in osmosis", *Science* 126, (1957), pp.252-253.
11) Ray, P.M., "On the theory of osmotic water movement", *Pant Physiol.* 35, (1960), pp.783-795.
12) Zhang, X., Curry, F.E. and Weinbaum, S., "Mechanism of osmotic flow in a periodic fiber array", *Am. J. Physiol.* 290, (2006), pp.H844-H852.
13) Yan, Z.Y., Weinbaum, S. and Pheffer, R., "On the fine structure of osmosis including three-dimensional pore entrance and exit behaviour", *J. Fluid Mech.* 162, (1986), pp.415-438.
14) Probstein, R.F., Physicochemical hydrodynamics, (A John Wiley & Sons, Inc. 2003).
15) Smith, F.G III and Deen, W.M., "Electrostatic double-layer interactions for spherical colloids in cylindrical pores", *J. Colloid Interface Sci.* 78,,(1980), pp. 444-465.
16) Bhalla, G. and Deen, W.M., "Effects of molecular shape on osmotic reflection coefficients", *J. Membrane Sci.* 306, (2007), pp.116-124.
17) Brenner, H. and Gaydos, L.J., "The constrained Brownian movement of spherical particles in cylindrical pores of comparable radius", *J. Colloid Interface Sci.* 58, (1977), pp.312-356.